PASJ: Publ. Astron. Soc. Japan , 1–??,
© 2010. Astronomical Society of Japan.

arXiv:1002.1853v1 [astro-ph.GA] 9 Feb 2010

Dense and Warm Molecular Gas and Warm Dust in Nearby Galaxies

Satoki Matsushita
Institute of Astronomy and Astrophysics, Academia Sinica, P.O. Box 23-141, Taipei 10617, Taiwan, R.O.C.
satoki@asiaa.sinica.edu.tw
Ryohei Kawabe
Nobeyama Radio Observatory, Minamimaki, Minamisaku, Nagano, 384-1305
Kotaro Kohno
Institute of Astronomy, University of Tokyo, 2-21-1 Osawa, Mitaka, Tokyo 181-0015
Tomoka Tosaki
Department of Geoscience, Joetsu University of Education, 1 Yamayashiki, Joetsu, Niigata, 043-8512
and
Baltasar Vila-Vilaró
ALMA Santiago / ESO, Av Apoquindo 3846, Piso 19, Las Condes, Santiago, Chile

(Received ; accepted)

Abstract

We performed ^{12}CO(1 – 0), ^{13}CO(1 – 0), and HCN(1 – 0) single-dish observations (beam size $\sim 14'' - 18''$) toward nearby starburst and non-starburst galaxies using the Nobeyama 45 m telescope. The ^{13}CO(1 – 0) and HCN(1 – 0) emissions were detected from all the seven starburst galaxies, with the intensities of both lines being similar (i.e., the ratios are around unity). On the other hand, for case of the non-starburst galaxies, the ^{13}CO(1 – 0) emission was detected from all three galaxies, while the HCN(1 – 0) emission was weakly or not detected in past observations. This result indicates that the HCN/^{13}CO intensity ratios are significantly larger ($\sim 1.15 \pm 0.32$) in the starburst galaxy samples than the non-starburst galaxy samples ($< 0.31 \pm 0.14$). The large-velocity-gradient model suggests that the molecular gas in the starburst galaxies have warmer and denser conditions than that in the non-starburst galaxies, and the photon-dominated-region model suggests that the denser molecular gas is irradiated by stronger interstellar radiation field in the starburst galaxies than that in the non-starburst galaxies. In addition, HCN/^{13}CO in our sample galaxies exhibit strong correlations with the IRAS 25 μm flux ratios. It is a well established fact that there exists a strong correlation between dense molecular gas and star formation activities, but our results suggest that molecular gas temperature is also an important parameter.

Key words: galaxies: ISM, galaxies: nuclei, galaxies: starburst, ISM: molecules

1. Introduction

Galaxies consist of vast numbers of stars formed from molecular clouds. It has therefore been suggested that the process of star formation in galaxies depends largely on the distribution, kinematics, and physical conditions of the molecular gas. One of the primary molecular gas properties critical to star formation is the number density. Observational studies of molecular clouds in our Galaxy suggest that stars are formed from the dense locale of molecular clouds, rather than the diffuse regions (e.g., Lada 1992). Extragalactic single-dish molecular gas observations indicate that the overall amount of dense molecular gas, which can be traced by the HCN(1 – 0) luminosity, is tightly correlated with the global star formation rate, which can in turn be traced by the far-infrared (FIR) luminosity observed with the Infrared Astronomical Satellite (IRAS) (Solomon et al. 1992; Gao & Solomon 2004a; Gao & Solomon 2004b). This correlation is much tighter than that between the diffuse molecular gas, or in other words, the total amount of molecular gas that can be traced by ^{12}CO(1 – 0), and the global star formation rate (e.g., Sanders et al. 1991; Young & Scoville 1991; Young et al. 1996; Gao & Solomon 2004b). In addition, Solomon et al. (1992) and Gao & Solomon (2004b) also raise the possibility of the fact that the HCN/^{12}CO luminosity ratio correlates well with the FIR/^{12}CO luminosity ratio, namely the fraction of dense molecular gas correlates well with the star formation efficiency, and this suggests that HCN/^{12}CO is a good indicator for star formation.

High spatial resolution interferometric observations toward the center of a galaxy with a high infrared luminosity indicate that extragalactic star forming regions coincide well with the distributions of dense molecular gas (HCN) (Kohno et al. 1999). The distributions of diffuse molecular gas (^{12}CO), on the other hand, only loosely match those of star forming regions. As a matter of fact, the HCN/^{12}CO integrated intensity ratios are high ($\sim 0.1 - 0.2$) in active star forming regions in the centers of galaxies with high infrared luminosity ($> 10^{10}$ L$_\odot$), but low (< 0.1) in the centers of galaxies with low star forming activities or post-starburst activities (Kohno et al. 1999; Reynaud & Downes 1999; Kohno et al. 2002). Star forming regions in the outer parts of galaxies, where normally have low

infrared luminosities or low star formation rate, have low HCN/^{12}CO at giant molecular cloud scale (Helfer & Blitz 1997; Brouillet et al. 2005). These results strongly imply that the density of molecular gas play a critical role in the active star formation phenomena.

The relation between star formation and temperature, another important molecular gas property, has so far not been well established. There are several surveys observing ^{12}CO(2 – 1) and ^{12}CO(1 – 0) lines toward galaxies with various star formation activities (such as starburst, interacting, and quiescent galaxies), and most of the surveys yield an average ^{12}CO(2 – 1)/(1 – 0) of around unity (Braine et al. 1993; Aalto et al. 1995; Hafok & Stutzki 2003). Surveys focusing on the ^{12}CO(3 – 2) and ^{12}CO(1 – 0) lines indicate that variations in ^{12}CO(3 – 2)/(1 – 0) tend to have somewhat larger dependence on star formation activities as compared to ^{12}CO(2 – 1)/(1 – 0); starburst galaxies tend to have higher ^{12}CO(3 – 2)/(1 – 0) of around unity, but normal galaxies tend to have lower ratio of around 0.5 or lower (Hafok & Stutzki 2003; Dumke et al. 2001; Devereux et al. 1994). These multi-transition ^{12}CO observations suggest that the ^{12}CO lines in nearby normal and starburst galaxies are optically thick, with a tendency to be saturated to unity, namely thermalized, in the vicinity of certain star formation activities. It is therefore difficult to deduce correlations between star formation activities and multi-transition ^{12}CO ratios.

The intensities of the ^{13}CO(1 – 0) lines, on the other hand, display more drastic changes than those of the ^{12}CO lines with respect to star formation activities. In merging galaxies, the ^{13}CO(1 – 0) intensities tend to be very low, and ^{12}CO(1 – 0)/^{13}CO(1 – 0) often exceed 20, in contrast to normal or starburst galaxies (not including extreme starbursts) that have an average value of ~ 10 (Aalto et al. 1991; Casoli et al. 1992; Aalto et al. 1995). However, this clear contrast in ^{12}CO(1 – 0)/^{13}CO(1 – 0) is only manifested between merging galaxies and normal/starburst galaxies, and there exists only a weak trend between normal and starburst galaxies as a function of dust temperature or the 60 μm and 100 μm FIR flux ratio (Sage & Isbell 1991; Aalto et al. 1991; Aalto et al. 1995).

In the study of M51 multi-line observations, we discovered an excellent density and temperature probe, the HCN(1 – 0)/^{13}CO(1 – 0) ratio (Matsushita et al. 1998, hereafter Paper I; Matsushita et al. 1999). The utility of this ratio has been confirmed by higher-J interferometric ^{12}CO observations (Matsushita et al. 2004).

In this paper, we present HCN(1 – 0), ^{13}CO(1 – 0), and ^{12}CO(1 – 0) observations toward galaxies with various levels of star formation activities, and discuss the relation between the physical conditions of molecular gas and the levels of star formation activities. In addition, we compare the IR properties of these galaxies, and show that the molecular gas and dust are localized in similar regions and strongly irradiated by the radiation from starburst regions.

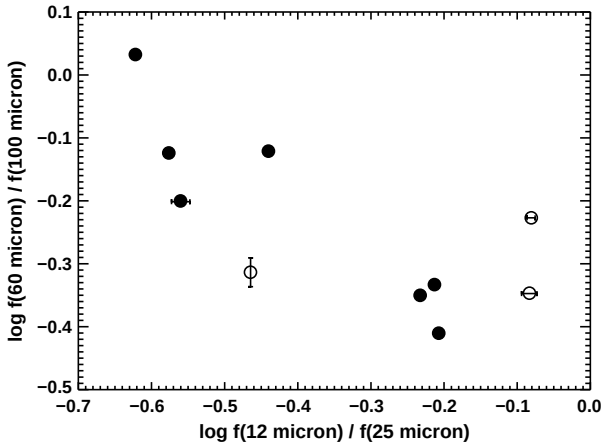

Fig. 1. Correlation diagrams between the $f(12\ \mu\mathrm{m})/f(25\ \mu\mathrm{m})$ and the $f(60\ \mu\mathrm{m})/f(100\ \mu\mathrm{m})$ IR flux ratios. Filled and open circles denote the starburst and the non-starburst galaxy samples, respectively. Our sample galaxies extend over a wide range of IR flux ratios reported in Helou (1986) and Dale et al. (2001), covering a wide spectrum of star formation activities.

2. Sample Galaxies

For this survey, we picked 7 starburst galaxies and 3 non-starburst galaxies so as to cover a wide range of star formation activities. We summarized the basic parameters of the starburst and non-starburst galaxy samples in Table 1 and Table 2, respectively. To ensure the wide spectrum of star formation activities of our samples, we plot the IR flux ratios between 12 μm and 25 μm, $f(12\ \mu\mathrm{m})/f(25\ \mu\mathrm{m})$, and that between 60 μm and 100 μm, $f(60\ \mu\mathrm{m})/f(100\ \mu\mathrm{m})$ in Fig. 1. It has well established that this correlation traces star formation activities (Helou 1986; Dale et al. 2001). Our sample galaxies extend over a wide range of the IR flux ratios, covering most of the range of the diagrams shown in Helou (1986) and Dale et al. (2001), thus ensuring the wide coverage of star formation activities.

2.1. Starburst Galaxy Sample

Among the starburst galaxy samples are M82, NGC 253, NGC 2146, NGC 3504, NGC 2903, NGC 6946, and NGC 6951, whose FIR luminosities are on the order of 10^{10} $L_\odot$ (Sanders et al. 2003).

M82 and NGC 253 exhibit energetic phenomena at various wavelengths, such as Hα, X-ray, and molecular gas outflows (e.g., Strickland et al. 2004; Nakai et al. 1987) and molecular superbubbles (e.g., Matsushita et al. 2005; Sakamoto et al. 2006). These galaxies are therefore known as prototypical starburst galaxies (e.g., Rieke et al. 1980; Rieke et al. 1988; Devereux 1989).

NGC 2146 and NGC 3504 display star formation activities comparable to M82 and NGC 253 on the basis of 1.65, 2.2, and 10 μm photometric observations (Devereux 1989; Devereux et al. 1994). In particular, NGC 2146 hosts a kpc-scale starburst-driven X-ray outflow (Armus

Table 1. Basic parameters of the starburst galaxy samples.

Galaxy	Type*	α(B1950)	δ(B1950)	Ref.†	Dist.‡	Ref.§	$L_{\rm FIR}$‖
NGC 253	SAB(s)c	$00^{\rm h}45^{\rm m}05\overset{\rm s}{.}63$	$-25°33'40\overset{''}{.}5$	1	3.5	8	10.29
NGC 2146	SB(s)ab pec	$06^{\rm h}10^{\rm m}41\overset{\rm s}{.}10$	$+78°22'28\overset{''}{.}1$	2	17.2	9	10.93
NGC 2903	SAB(rs)bc	$09^{\rm h}29^{\rm m}20\overset{\rm s}{.}26$	$+21°43'20\overset{''}{.}74$	3	8.9	10	10.05
M82	I0 sp	$09^{\rm h}51^{\rm m}43\overset{\rm s}{.}5$	$+69°55'00\overset{''}{.}0$	4	3.9	11	10.61
NGC 3504	(R)SAB(s)ab	$11^{\rm h}00^{\rm m}28\overset{\rm s}{.}53$	$+28°14'31\overset{''}{.}2$	5	26.5	9	10.56
NGC 6946	SAB(rs)cd	$20^{\rm h}33^{\rm m}49\overset{\rm s}{.}2$	$+59°58'49\overset{''}{.}5$	6	5.9	12	10.01
NGC 6951	SAB(rs)bc	$20^{\rm h}36^{\rm m}36\overset{\rm s}{.}59$	$+65°55'46\overset{''}{.}0$	7	26.8	13	10.46

Notes.
* Morphological type taken from RC3.
† References for the positions.
‡ Distance in Mpc.
§ References for distance.
‖ Far infrared luminosity taken from Sanders et al. (2003).
References — (1) Keto et al. (1993). (2) Condon et al. (1982). (3) 2.2 μm peak of Wynn-Williams & Becklin (1985). (4) Shen & Lo (1995). (5) Condon et al. (1990). (6) Turner & Ho (1983). (7) Saikia et al. (1994). (8) Rekola et al. (2005). (9) Tully (1988). (10) Drozdovsky & Karachentsev (2000). (11) Sakai & Madore (1999). (12) Karachentsev et al. (2000). (13) Valentini et al. (2003).

et al. 1995; Della Ceca et al. 1999; Inui et al. 2005) and molecular outflow and superbubbles (Tsai et al. 2009) from the central region, which are similar to those in M82 or NGC 253, and therefore strongly support the existence of ongoing starburst.

NGC 2903 is one of the Sérsic-Pastoriza galaxies (a catalogue of galaxies with peculiar or complex nuclei such as "hot spots" or "amorphous nucleus"; Sérsic & Pastoriza 1965; Sérsic & Pastoriza 1967; Sérsic 1973) and its nuclear appearance is classified as "hot spots". This nuclear "hot spots" region is a powerful IR source, and it has been proposed that this phenomenon could be the result of a starburst (Rieke et al. 1980; Telesco & Harper 1980), a conjecture that has been supported by radio and IR observations (Wynn-Williams & Becklin 1985; Alonso-Herrero et al. 2001).

NGC 6946 is a large spiral galaxy with a small nuclear bar (Elmegreen et al. 1998) and ongoing nuclear starburst (Turner & Ho 1983; Engelbracht et al. 1996).

NGC 6951 is also a Sérsic-Pastoriza galaxy, with a circumnuclear "hot spots" ring (Barth et al. 1995; Elmegreen et al. 1999). This ring is bright in Hα (Wozniak et al. 1995; González-Delgado et al. 1997) and exhibits high star formation rate (SFR) of $\sim 3-4$ M$_\odot$ yr^{-1} as well as high star formation efficiency (SFE), comparable to those in the central regions of nearby starburst galaxies (Kohno et al. 1999; Wozniak et al. 1995).

2.2. Non-Starburst Galaxy Sample

The non-starburst galaxy sample consists of NGC 4736, NGC 4826, and NGC 5195, whose FIR luminosities are around 10^9 L$_\odot$ (Sanders et al. 2003).

The optical spectra of the nuclear regions of both NGC 4736 and NGC 5195 exhibit strong Balmer absorption lines (Ho et al. 1995; Taniguchi et al. 1996; Sauvage et al. 1996; Greenawalt et al. 1998). Since these strong Balmer absorption lines are typically found in the spectra of A-type stars, stellar populations of galaxies with such absorption lines are believed to be dominated by A-type stars. Indeed, the stellar population synthesis analysis implies that the dominant stellar populations of NGC 4736 and NGC 5195 extend up to at most A4 to A7, and that the optical light is dominated by these stellar populations (Pritchet 1977; Warner 1974). The likely mechanism for the creation of "A-type star dominated" galaxies is as follows: Starburst phenomena produce enormous numbers of early to late-type stars, assuming a general initial mass function. Early-type stars (OB stars) live at most 10^8 years, so that at the time 10^9 years after the beginning of the starburst, the early-type stars are burned out, with vast numbers of A-type stars remaining. Therefore, galaxies with numerous A-type stars can be considered post-starburst galaxies (Rieke 1988; Rieke et al. 1988; Walker et al. 1988). Molecular gas observations support the hypothesis that, in the Balmer absorption dominated regions, there is little molecular gas (Tosaki & Shioya 1997). In some cases, molecular gas exists in the "A-type star dominated" galaxies, but it is stable against gravitational instability (Shioya et al. 1998; Kohno et al. 2002) with almost no high-density gas present (Kohno 1998; Kohno et al. 2002). Therefore, we classified NGC 4736 and NGC 5195 as "post-starburst" as in other articles.

NGC 4826 is classified as a type 2 transition object (the [O I] line from the nucleus has a strength intermediate between those of H II nuclei and LINERs; Ho et al. 1997). Even if all of the Hα emission of this galaxy originates in the star forming regions, the extinction corrected total Hα luminosity, L(Hα), of 5.7×10^{40} erg s^{-1} (Young et al. 1996) indicates a SFR of only ~ 0.45 M$_\odot$ yr^{-1}, using the relationship between the SFR and the L(Hα) (Kennicutt 1998). Hence this galaxy can be safely regarded as a non-starburst galaxy.

3. Observations

Observations of the central regions of the sample galaxies using the Nobeyama 45 m telescope were carried out in the HCN(1 – 0), ^{13}CO(1 – 0), and ^{12}CO(1 – 0) lines (rest

Table 2. Basic parameters of the non-starburst galaxy samples.

Galaxy	Type*	α(B1950)	δ(B1950)	Ref.†	Dist.‡	Ref.§	Activity‖	$L_{\rm FIR}$#
NGC 4736	(R)SA(r)ab	$12^{\rm h}48^{\rm m}31\overset{\rm s}{.}910$	$+41°23'31\overset{''}{.}78$	1	4.3	3	Post-SB	9.59
NGC 4826	(R)SA(rs)ab	$12^{\rm h}35^{\rm m}16\overset{\rm s}{.}07$	$+21°57'13\overset{''}{.}5$	2	4.1	3	T2	8.98
NGC 5195	I0 pec	$13^{\rm h}27^{\rm m}53\overset{\rm s}{.}27$	$+47°31'25\overset{''}{.}5$	2	8.4	4	Post-SB	9.44:

Notes.
* Morphological type taken from RC3.
† References for the positions.
‡ Distance in Mpc.
§ References for distance.
‖ Star formation activity. "SB" and "T2" denote starburst and type 2 transition object, respectively. See text for details.
Far infrared luminosity taken from Sanders et al. (2003). A value with a colon (":") indicates that the value has a large uncertainty.
References — (1) Turner & Ho (1994). (2) Hummel et al. (1987). (3) Tully (1988). (4) Feldmeier et al. (1997).

frequency = 86.632 GHz, 110.201 GHz, and 115.271 GHz, respectively). We observed ^{13}CO(1 – 0) and HCN(1 – 0) simultaneously for the starburst samples during 1997 February – April, 1997 December, and 1999 March – April (the 1999 observation run was only for NGC 6951). The ^{13}CO(1 – 0) and ^{12}CO(1 – 0) simultaneous observations for the non-starburst samples and M82 were performed during 1998 March – April.

Two SIS receivers, S100 and S80, were used, and these were tuned to the ^{13}CO(1 – 0) and HCN(1 – 0) lines, respectively, for the ^{13}CO and HCN simultaneous observations. The half power beam widths (HPBW) for the ^{13}CO and HCN simultaneous observations (except for NGC 6951) were 15″ and 17″, and the main-beam efficiencies, $\eta_{\rm mb}$, were 0.51 ± 0.03 and 0.47 ± 0.02, respectively. In case of NGC 253, we applied $\eta_{\rm mb}$ of 0.48 and 0.35, respectively, due to the low declination (and therefore the low elevation at the telescope site) of this source. The HPBW for the NGC 6951 observations were 15″ and 18″, and $\eta_{\rm mb}$ were 0.48 ± 0.02 and 0.49 ± 0.02, respectively. The differences in the HPBW and $\eta_{\rm mb}$ from other observations are due to the different observation year for this galaxy.

For the ^{12}CO(1 – 0) and ^{13}CO(1 – 0) simultaneous observations, S100 and S80 were tuned to ^{12}CO and ^{13}CO, respectively. Since the different (S80 instead of S100) receiver was used for the ^{13}CO line, the HPBW and $\eta_{\rm mb}$ were different from the ^{13}CO and HCN simultaneous observations; the HPBW for the ^{13}CO and ^{12}CO simultaneous observations were both 14″, and the $\eta_{\rm mb}$ were 0.40 ± 0.03 and 0.51 ± 0.03, respectively.

The telescope pointing was checked and corrected every hour, and the absolute pointing errors were less than 4″ during the observations. Due to the use of two SIS receivers, there were no relative pointing offsets between two simultaneously observed lines. The single side-band system noise temperatures at 87 GHz, 110 GHz, and 115 GHz throughout the observations were 200 – 400 K, 300 – 1400 K, and 600 – 1800 K, respectively. As back-ends, we used 2048-channel wide band acousto-optical spectrometers (AOS), with a total bandwidth of 250 MHz, corresponds to 650 km s^{-1} at the ^{12}CO(1 – 0) frequency. The line intensity calibration was accomplished by the chopper-wheel method (Ulich & Haas 1976), and the relative intensity errors were calibrated at every observation with the intensity of W51 main for NGC 6951 and IRC+10216 for the rest of the observations.

We observed the central regions of sample galaxies pointed toward the nuclei except for M82. M82 was observed toward five points for the ^{13}CO(1 – 0) and HCN(1 – 0) lines, and three points for the ^{12}CO(1 – 0) line. The observed positions are shown in Fig. 2 and Table 3. The positions (0″, 0″), (−15″, −3″), and (10″, 6″) are the so-called the nucleus, the South-West (SW) lobe, and the North-East (NE) lobe, respectively (e.g., Shen & Lo 1995).

The data were reduced using the reduction software package NEWSTAR of the Nobeyama Radio Observatory. The baselines of raw spectra were subtracted by fitting linear lines, or if necessary, second order polynomials. The line-free velocity range for each galaxy was defined with avoiding the line emission velocity range based on the previously published CO observations. The raw spectra with higher order baseline fluctuation were not used in our final spectra.

4. Results

The parameters of the observed lines from all of the sample galaxies (peak main beam brightness temperature, $T_{\rm MB}$, and integrated intensity, I) are summarized in Table 3, and the calculated integrated intensity ratios are summarized in Table 4. Since we did not observe the ^{12}CO(1 – 0) line for the starburst galaxy samples other than M82 and the HCN(1 – 0) line for the non-starburst galaxy samples, we made use instead of the data taken with the Nobeyama 45 m telescope from various published papers (see notes in Table 4).

Fig. 2 shows the ^{12}CO, ^{13}CO, and HCN line spectra toward the observed positions of the central region of M82, one of the starburst galaxy samples. The overall line shapes of each positions are similar across these three line spectra. The line shapes of all three spectra at the nucleus indicate constant brightness temperatures around the line center, $V_{\rm LSR} \sim 150 - 300$ km s^{-1}. It is also obvious that the ^{13}CO line is weaker than other two lines. On the other hand, the line shapes at the off-center indicate peak structures, and the peak brightness temperatures of the NE and SW lobes exceed those of the nucleus in all the observed lines. We did not detect the HCN line in the

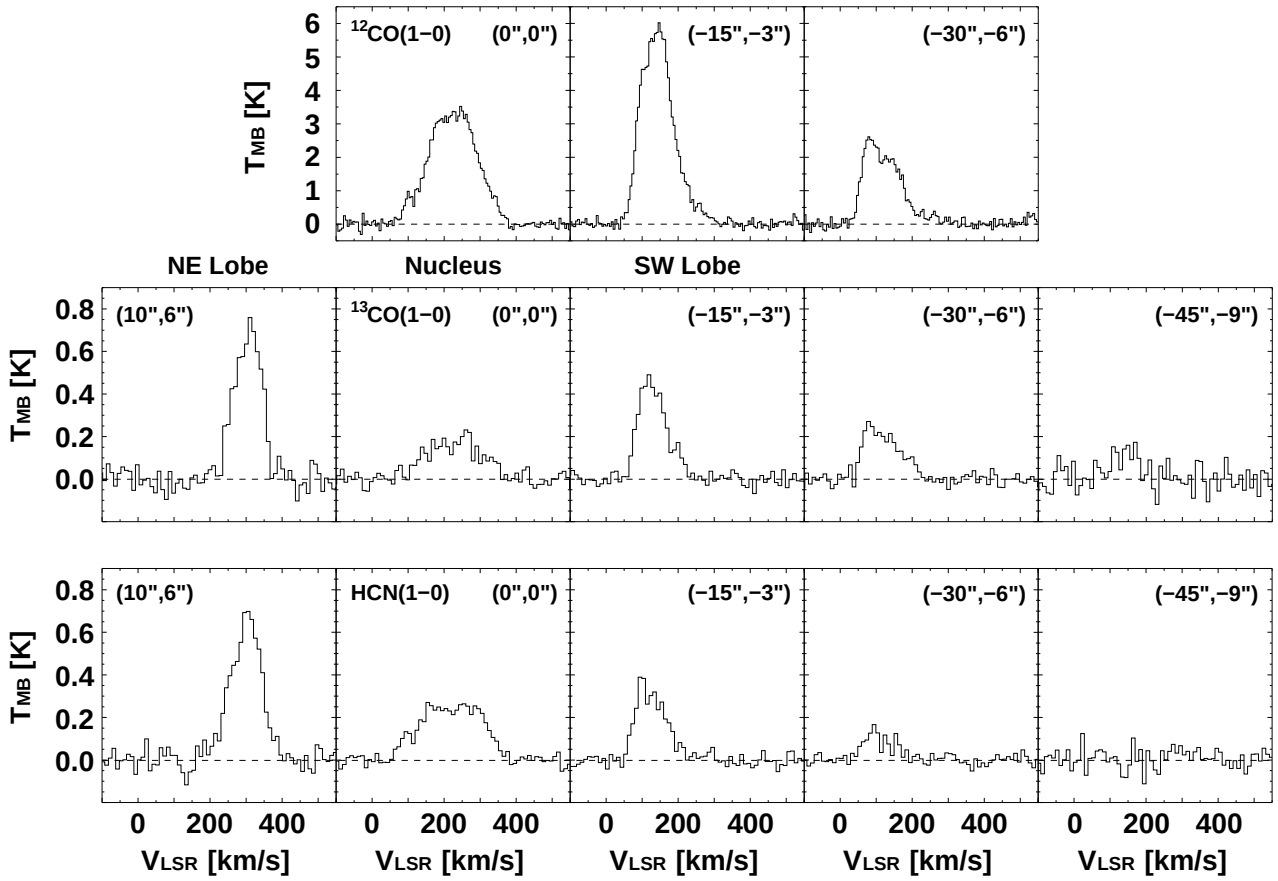

Fig. 2. ^{12}CO(1 – 0) (top row), ^{13}CO(1 – 0) (middle row), and HCN(1 – 0) (bottom row) spectra of the central region of the prototypical starburst galaxy M82. The horizontal axis is the LSR velocity, $V_{\rm LSR}$, and the vertical axis is the main beam temperature, $T_{\rm MB}$. The reference point ($0''$, $0''$) is the position of the galactic nucleus as determined from the peak of the 2.2 μm source (see Table 1). The other points are in R.A. and Decl. offset from the reference point.

farthest observed region, ($-45''$, $-9''$). The line intensity ratios are, on the other hand, different from the brightness temperature distributions. At the center of M82, the intensity ratios (HCN/^{13}CO, ^{12}CO/^{13}CO, and HCN/^{12}CO) are all high, but these ratios gradually decrease with increasing offsets from the center (Table 4).

Fig. 3 shows ^{13}CO(1 – 0) and HCN(1 – 0) line spectra of the other starburst galaxy samples. Both lines have similar line shapes and intensities for all galaxies, which is similar to those for the central $\pm 15''$ region of M82. We note again that since the HCN and ^{13}CO lines were observed simultaneously, there is no HCN/^{13}CO integrated intensity ratio errors due to the relative pointing offsets.

Fig. 4 shows the ^{13}CO(1 – 0) and ^{12}CO(1 – 0) line spectra of the non-starburst galaxy samples. The integrated intensity of ^{12}CO(1 – 0) line, I(^{12}CO), for NGC 4736 is consistent with that of Kohno (1998). For I(^{12}CO) of NGC 4826, it is 67% of the value obtained by Kohno (1998). This disagreement may be explained by pointing error and/or calibration error. The pointing error of our observations was $\sim 4''$, larger than the $\sim 2''$ of Kohno (1998). On the other hand, Kohno (1998) did not observe any intensity calibrator as we did with IRC+10216. For I(^{12}CO) of NGC 5195, we only detect 46% of the value obtained by Kohno et al. (2002). This is because we had mistakenly placed the off-position of the position switching observations at NGC 5194, which is the counterpart of the M51 interaction system for NGC 5195 and rich in molecular gas. This can be seen as the absorption-like feature around the velocity range of $500 - 550$ km s^{-1} in Fig. 4, which did not show up in the spectrum of Kohno et al. (2002). Therefore we use the derived HCN/^{13}CO value for NGC 5195 as an upper limit.

The HCN/^{13}CO integrated intensity ratios between the starburst and non-starburst galaxy samples are significantly different: We obtained an average HCN/^{13}CO toward the nuclei of the starburst samples of 1.15 ± 0.32, and a value of 1.10 ± 0.30 for starburst samples including the off-center starburst regions of M82, namely the NE and SW lobes. The average HCN/^{13}CO ratio toward the nuclei of the non-starburst galaxy samples and that including the non-starburst regions of M82, namely ($-30''$, $-6''$) and ($-45''$, $-9''$), are $< 0.31 \pm 0.14$ and $< 0.32 \pm 0.12$, respectively. These values are consistent with previously published results: Paper I suggests that starburst regions tend to have higher HCN/^{13}CO of > 1, but less active star

Table 3. Observed properties for sample galaxies.

Galaxy	Position*	$T_{\rm MB}(^{12}{\rm CO})^{\dagger}$	$T_{\rm MB}(^{13}{\rm CO})^{\dagger}$	$T_{\rm MB}({\rm HCN})^{\dagger}$	$I(^{12}{\rm CO})^{\ddagger}$	$I(^{13}{\rm CO})^{\ddagger}$	$I({\rm HCN})^{\ddagger}$
NGC 253	(0″, 0″)	—	0.43 ± 0.03	0.42 ± 0.02	—	168 ± 15	258 ± 22
NGC 2146	(0″, 0″)	—	0.074 ± 0.015	0.072 ± 0.007	—	16.0 ± 1.3	12.3 ± 0.7
NGC 2903	(0″, 0″)	—	0.074 ± 0.008	0.066 ± 0.009	—	9.1 ± 0.7	9.8 ± 0.6
M82	(0″, 0″)	3.52 ± 0.08	0.23 ± 0.03	0.27 ± 0.02	565 ± 33	34.5 ± 2.6	55.4 ± 2.6
(NE lobe)	(+10″, +6″)	—	0.76 ± 0.04	0.70 ± 0.04	—	66.1 ± 4.4	71.2 ± 3.6
(SW lobe)	(−15″, −3″)	6.02 ± 0.13	0.49 ± 0.03	0.39 ± 0.03	646 ± 38	45.2 ± 2.9	36.2 ± 1.9
	(−30″, −6″)	2.61 ± 0.33	0.27 ± 0.05	0.17 ± 0.02	288 ± 20	29.0 ± 2.8	12.2 ± 0.9
	(−45″, −9″)	—	0.17 ± 0.05	< 0.08	—	12.7 ± 2.2	< 3.2
NGC 3504	(0″, 0″)	—	0.052 ± 0.005	0.060 ± 0.009	—	7.7 ± 0.5	10.1 ± 0.6
NGC 6946	(0″, 0″)	—	0.152 ± 0.012	0.151 ± 0.008	—	21.9 ± 1.4	21.4 ± 1.0
NGC 6951	(0″, 0″)	—	0.055 ± 0.009	0.034 ± 0.007	—	8.1 ± 0.6	6.1 ± 0.5
NGC 4736	(0″, 0″)	0.26 ± 0.01	0.043 ± 0.012	—	44.1 ± 2.7	6.3 ± 1.4	—
NGC 4826	(0″, 0″)	0.53 ± 0.05	0.11 ± 0.03	—	87.0 ± 5.9	17.2 ± 3.6	—
NGC 5195	(0″, 0″)	0.26 ± 0.04	0.10 ± 0.02	—	37.9 ± 2.8	12.0 ± 2.2	—

Notes.
* Offset from the position of the nucleus indicated in Tables 1 and 2.
† Peak main-beam temperature in K. Quoted uncertainties are 1σ and upper limits are 2σ.
‡ Integrated intensity in K km s^{-1}. We define the integrated intensity as $I = \int T_{\rm MB} dv$. Quoted uncertainties are 1σ and upper limits are 2σ.

Table 4. Integrated intensity ratios for sample galaxies.

Galaxy	Position*	HCN/^{13}CO†	^{12}CO/^{13}CO†	HCN/^{12}CO†
NGC 253	(0″, 0″)	1.53 ± 0.19	$7.4 \pm 0.6^{\|}$	$0.209 \pm 0.018^{\|}$
NGC 2146	(0″, 0″)	0.77 ± 0.08	$11.8 \pm 1.0^{\#}$	$0.065 \pm 0.004^{\#}$
NGC 2903	(0″, 0″)	1.08 ± 0.11	$11.3 \pm 0.9^{**}$	$0.095 \pm 0.006^{**}$
M82	(0″, 0″)	1.61 ± 0.14	16.4 ± 1.6	0.098 ± 0.007
(NE lobe)	(+10″, +6″)	1.08 ± 0.09	—	—
(SW lobe)	(−15″, −3″)	0.80 ± 0.07	14.3 ± 1.2	0.056 ± 0.004
	(−30″, −6″)	0.42 ± 0.05	9.9 ± 1.2	0.042 ± 0.004
	(−45″, −9″)	< 0.25	—	—
NGC 3504	(0″, 0″)	1.32 ± 0.12	$8.8 \pm 0.6^{\dagger\dagger}$	$0.094 \pm 0.008^{\dagger\dagger}$
NGC 6946	(0″, 0″)	0.98 ± 0.08	$9.7 \pm 0.6^{\#}$	$0.101 \pm 0.005^{\#}$
NGC 6951	(0″, 0″)	0.75 ± 0.08	$6.0 \pm 0.5^{**}$	$0.125 \pm 0.010^{**}$
NGC 4736	(0″, 0″)	$< 0.32^{\ddagger}$	7.0 ± 1.6	$< 0.042^{\ddagger}$
NGC 4826	(0″, 0″)	$0.48 \pm 0.10^{\ddagger}$	5.0 ± 1.1	$0.063^{\ddagger}$
NGC 5195	(0″, 0″)	$< 0.13 \pm 0.06^{\S}$	3.2 ± 0.6	$0.018 \pm 0.007^{\S}$

Notes.
* Offset from the position of the nucleus indicated in Tables 1 and 2.
† Ratio of integrated intensity indicated in Table 3. Integrated intensity that is not in Table 3 is taken from previously published papers, as indicated below. Quoted uncertainties are 1σ, and upper limits are 2σ, except for the HCN/^{13}CO value of NGC 5195 (see note § below).
‡ HCN(1 – 0) integrated intensity and HCN/^{12}CO ratio taken from Kohno (1998).
§ HCN(1 – 0) integrated intensity and HCN/^{12}CO ratio taken from Kohno et al. (2002). Due to the off-position problem, we take HCN/^{13}CO as an upper limit (see Sect.4 for detail).
‖ ^{12}CO integrated intensity taken from Sorai et al. (2000).
^{12}CO integrated intensity taken from Sorai et al. (2002).
** ^{12}CO integrated intensity taken from Kuno et al. (2007).
†† ^{12}CO integrated intensity taken from Kuno et al. (2000).

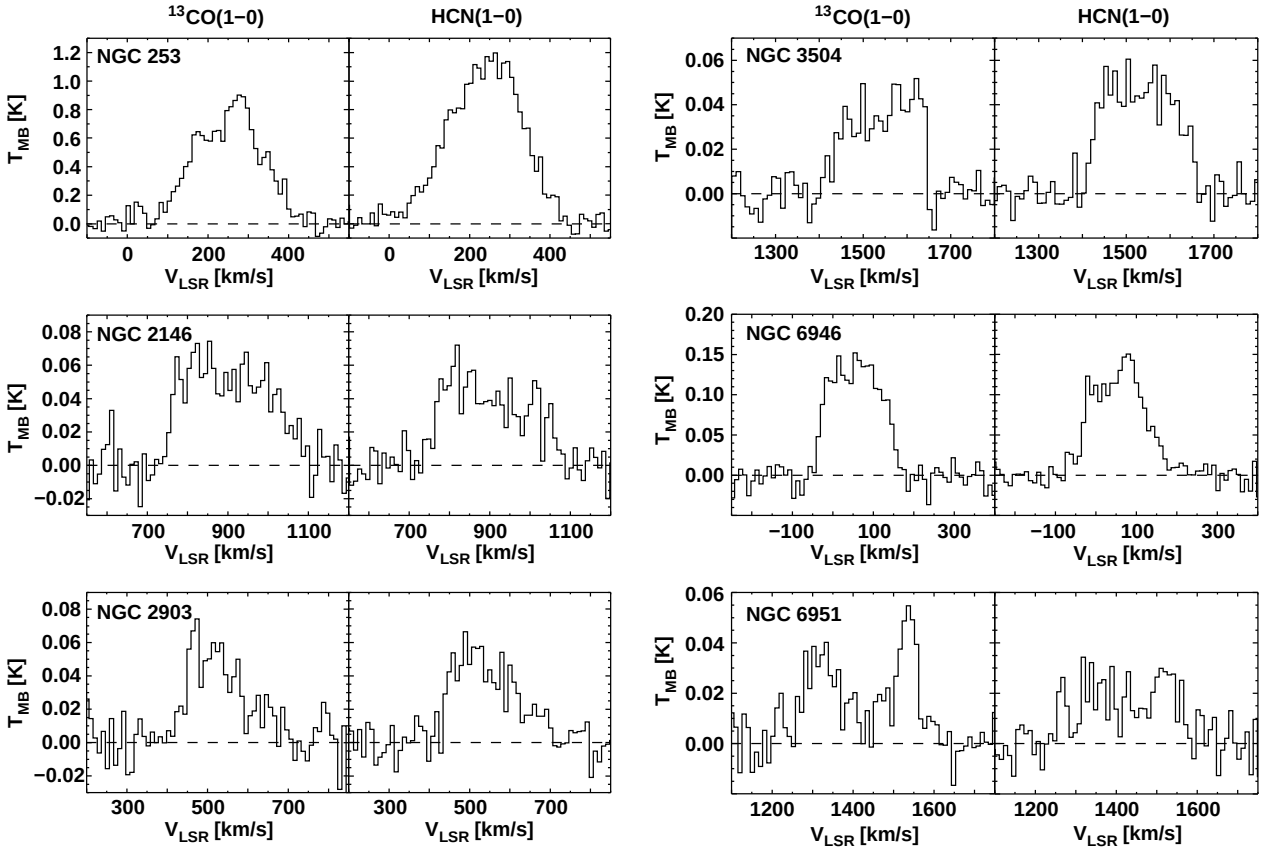

Fig. 3. ^{13}CO(1 – 0) and HCN(1 – 0) spectra toward the center of the starburst galaxy samples. Two spectra are shown for each galaxy; the spectrum on the left-hand side denotes the ^{13}CO(1 – 0) line, and that on the right-hand side denotes the HCN(1 – 0) line. The horizontal and vertical axes are $V_{\rm LSR}$ and $T_{\rm MB}$, respectively. Note that the scale for the vertical axis is the same for the ^{13}CO and HCN spectra.

forming regions tend to have lower ratios ($\lesssim 1$). Note that the results of Paper I is based on interferometric observations; therefore it is sensitive to compact components, such as high density gas (i.e., HCN). It follows that ratios in Paper I are bound to take on larger values than those in this paper, which is based on single-dish observations.

The ^{12}CO/^{13}CO and HCN/^{12}CO integrated intensity ratios between starburst and non-starburst galaxy samples also show differences with the average values for the starburst samples larger than those for the non-starburst samples: The average ^{12}CO/^{13}CO integrated intensity ratios toward the nuclei of the starburst and non-starburst samples are 10.2 ± 3.2 and 5.1 ± 1.6, respectively, and the average HCN/^{12}CO integrated intensity ratios for these samples are 0.11 ± 0.04 and $< 0.04 \pm 0.02$, respectively.

All the HCN/^{13}CO, ^{12}CO/^{13}CO, and HCN/^{12}CO ratios for the starburst galaxy samples are $2-3$ times larger than those for the non-starburst galaxy samples. These results suggest that the conditions of molecular gas in the starburst regions differ significantly from those in the non-starburst regions.

5. Discussions

5.1. Physical Conditions of Molecular Gas in Sample Galaxies

Using the line ratios derived above, we can estimate the physical conditions of molecular gas in our starburst and non-starburst sample galaxies. To that end, we make use of the large-velocity-gradient (LVG) approximation (Goldreich & Kwan 1974; Scoville & Solomon 1974) assuming a one-zone model, and the photon dominated region (PDR) model (Meijerink & Spaans 2005; Meijerink et al. 2007). Note that the estimated physical conditions are averaged values within one beam size of our observations, which corresponds to a few hundred to a few kpc scale in linear size. Although deriving an averaged value within one beam is extremely simplified assumption compared to the real situations of molecular clouds and radiation fields in galaxies, it is successfully derived in various galaxies in the past studies. The overlapping effect of molecular clouds is expected to be small, based on the small shadowing effect in molecular clouds of our Galaxy that is edge-on (Burton & Gordon 1978), so we assume that we see most of the emission from each molecular clouds in our beam, and therefore it is safe to use the LVG and PDR models

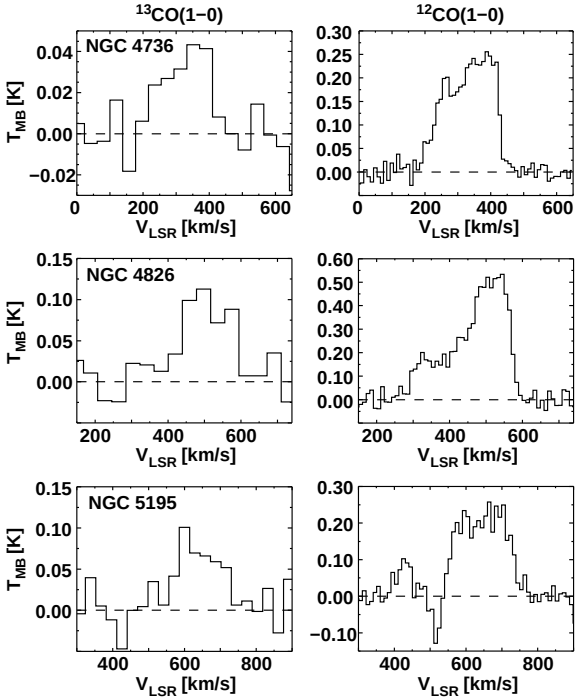

Fig. 4. ^{13}CO(1 – 0) and ^{12}CO(1 – 0) spectra toward the center of non-starburst galaxy samples. Two spectra are shown for each galaxy; the spectrum on the left-hand side denotes the ^{13}CO(1 – 0) line, and that on the right-hand side denotes the ^{12}CO(1 – 0) line. The horizontal and vertical axes are $V_{\rm LSR}$ and $T_{\rm MB}$, respectively.

in our datasets.

Spergel & Blitz (1992) suggested that the increase of the HCN intensity toward the centers of galaxies can be due to the increase of gas pressure, not due to the increase of gas density induced by gravitational instability. Hence, they predicted that larger galaxies should have stronger HCN intensities than those in smaller galaxies. This prediction can be rejected from the comparison of the HCN/^{12}CO and HCN/^{13}CO ratios between our Galaxy and M82: Our Galaxy, which is a larger galaxy, has the HCN/^{12}CO and HCN/^{13}CO ratios of ~ 0.08 (Jackson et al. 1996; Helfer & Blitz 1997) and ~ 0.8 (Matsushita et al. 1998), respectively, at the Galactic center. The center of a much smaller galaxy, M82, has much larger HCN/^{12}CO and HCN/^{13}CO ratios of ~ 0.1 and ~ 1.6, respectively. Similar conclusion is also obtained by Gao & Solomon (2004b). We therefore assume that the differences of ratios between galaxies and within galaxies are due to the differences in physical conditions of molecular gas, not due to the differences in gas pressure.

5.1.1. LVG Model

The line intensity ratios for CO and HCN molecules under the LVG model were tabulated as a function of the kinetic temperatures, $T_{\rm k}$, from 10 K to 1000 K, and the H_2 number density, $n(H_2)$, from 10^1 cm^{-3} to 10^6 cm^{-3} for HCN(1 – 0)/^{13}CO(1 – 0), ^{12}CO(1 – 0)/^{13}CO(1 – 0), and HCN(1 – 0)/^{12}CO(1 – 0). The collision rates for CO molecules ≤ 250 K and ≥ 500 K were taken from Flower & Launay (1985) and McKee et al. (1982), respectively. The corresponding values for HCN molecules < 100 K and ≥ 100 K are available from Green & Thaddeus (1974) and on-line*. We fixed the abundances to the 'standard' relative abundance where $Z(^{13}{\rm CO}) = [^{13}{\rm CO}]/[{\rm H_2}] = 1 \times 10^{-6}$ (Solomon et al. 1979), $Z({\rm HCN}) = [{\rm HCN}]/[{\rm H_2}] = 2 \times 10^{-8}$ (Irvine et al. 1987), and $[^{12}{\rm CO}]/[^{13}{\rm CO}] = 50$. We also set the velocity gradient, dv/dr, to a fixed general value of 1.0 km s^{-1} pc^{-1}. The tabulated results are shown in Fig. 5.

The LVG calculations show that high HCN/^{13}CO ratio ($\gtrsim 1$) can be obtained under high density ($n(H_2) \sim 10^{5\pm1}$ cm^{-3}) and high temperature ($T_{\rm k} \gtrsim 50$ K) conditions. The calculations for ^{12}CO/^{13}CO show that high ratio (> 10) can be obtained under high density ($n(H_2) \sim 10^{4\pm1}$ cm^{-3}) and high temperature ($T_{\rm k} > 100$ K) conditions, or low density ($n(H_2) \lesssim 10^2$ cm^{-3}) conditions. The HCN/^{12}CO ratio, on the other hand, only traces the density, and a high ratio ($\gtrsim 0.1$) indicates high density ($n(H_2) > 2 \times 10^3$ cm^{-3}) condition. These results can be explained as follows: At high temperature, the energy distribution of the ^{13}CO rotational transition populating higher levels due to the low abundance and small dipole moment of the ^{13}CO molecules, and therefore the ^{13}CO(1 – 0) line will be optically thin with a corresponding decrease in the line intensity. On the other hand, ^{12}CO molecules are abundant and HCN molecules possess large dipole moments, therefore the ^{12}CO(1 – 0) and HCN(1 – 0) lines remain optically thick even under high temperature conditions. In terms of density, the HCN molecule has a high critical density, meaning that high density is a prerequisite condition for line emission. The ^{12}CO and ^{13}CO molecules have the same critical density but ^{12}CO emits under lower density conditions due to its abundance.

^{13}CO deficiency is often cited in the case of merging galaxies (i.e., extreme starburst galaxies; e.g., Aalto et al. 1991; Casoli et al. 1992). Our sample galaxies do not exhibit such extreme starburst behaviors, but the possibility of low $Z(^{13}{\rm CO})$ cannot be ruled out. In addition, starburst galaxies may have larger velocity gradients due to the large turbulences caused by active star formation. In this study, we checked the dependence of $Z(^{13}{\rm CO})$ and the velocity gradient with our LVG calculation results: If $Z(^{13}{\rm CO})$ is a factor of two lower than the standard abundance, or if the velocity gradient is a factor of two higher than the standard value we assumed above, the LVG calculations for ^{12}CO/^{13}CO and HCN/^{13}CO give rise to a temperature a factor of two lower.

Using the LVG calculations shown in the figure, we arrived at the physical conditions of molecular gas in the sample galaxies and summarized them in Table 5. Many of the starburst galaxy samples display high density ($> 5 \times 10^3$ cm^{-3}) and high temperature (> 100 K). But some of the galaxies (NGC 2146 and NGC 6951) have been estimated as rather lower density or temperature due

* The data are available at http://data.giss.nasa.gov/mcrates/data/hcn_he_rates.txt.

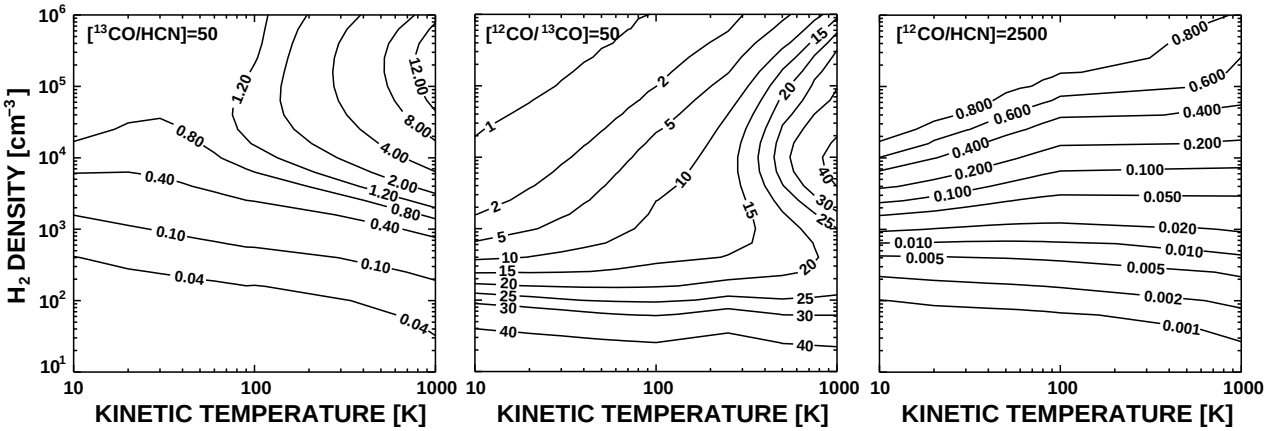

Fig. 5. H_2 number density (vertical axis) and kinetic temperature (horizontal axis) dependence of the HCN(1 – 0)/^{13}CO(1 – 0) (left), ^{12}CO(1 – 0)/^{13}CO(1 – 0) (middle), and HCN(1 – 0)/^{12}CO(1 – 0) (right) intensity ratios derived using the LVG calculations. Refer to the main text for the details of the calculations.

Table 5. Physical conditions of molecular gas in the sample galaxies based LVG calculations.

Galaxy	Position*	$n(H_2)^\dagger$	$T_k^\ddagger$
NGC 253	(0″, 0″)	$\sim(1-2)\times10^4$	$100-200$
NGC 2146	(0″, 0″)	$\sim(3-5)\times10^3$	$100-200$
NGC 2903	(0″, 0″)	$\sim(6-9)\times10^3$	$100-200$
M82	(0″, 0″)	$\sim(6-9)\times10^3$	$200-300$
(NE lobe)	(+10″, +6″)	$\sim4\times10^{4\pm1}$	$\gtrsim50$
(SW lobe)	(−15″, −3″)	$\sim(3-5)\times10^3$	~200
	(−30″, −6″)	$\sim(2-3)\times10^3$	~100
	(−45″, −9″)	$\lesssim5\times10^3$	—
NGC 3504	(0″, 0″)	$\sim1\times10^4$	~200
NGC 6946	(0″, 0″)	$\sim(6-9)\times10^3$	$100-200$
NGC 6951	(0″, 0″)	$\sim(6-9)\times10^3$	$60-100$
NGC 4736	(0″, 0″)	$\lesssim2\times10^3$	$\lesssim60$
NGC 4826	(0″, 0″)	$\sim(3-4)\times10^3$	$\sim50-60$
NGC 5195	(0″, 0″)	$\sim1\times10^3$	$\sim10-20$

Notes.
* Offset from the position of the nucleus indicated in Tables 1 and 2.
† Molecular hydrogen number density in cm^{-3}.
‡ Kinetic temperature in K.

to lower HCN/^{13}CO values, even these galaxies have high infrared luminosities (see Table 1). This is probably because of the larger distances of these galaxies than other nearby galaxies: Due to larger distances, the beam observes larger radius, where usually dominated by low density and low temperature materials, than other nearby galaxies, and therefore the beam averaged physical conditions exhibit lower values than other nearby galaxies. On the other hand, the non-starburst galaxy samples displays lower densities and temperatures of $n(H_2)\lesssim4\times10^3$ cm^{-3} and $T_k\lesssim60$ K than the starburst galaxy samples, even non-starburst samples located nearby.

We then compared our estimations with previously published values. In the case of M82, a region of higher density ($\sim4\times10^{4\pm1}$ cm^{-3}) can be observed at the NE lobe, which gradually tapers off toward the southwestern side of the galaxy. This trend, as well as the corresponding derived values, are very similar to those derived by Petitpas & Wilson (2000). The temperature, on the other hand, has high values ($200-300$ K) at the nucleus and the SW lobe, and ~100 K at the position (−30″, −6″). The decrease of the temperature as a function of radius in M82 (and in other galaxies) is also suggested from the ^{12}CO/^{13}CO observations (Paglione et al. 2001). The temperature of the NW lobe is not well constrained, $\gtrsim50$ K, and there exists no constraint for the position (−45″, −9″) due to the absence of ^{12}CO(1 – 0) data. These estimated temperatures and densities tend to be higher than those derived using various CO lines (including isotopes) observed with an interferometer (Weiß et al. 2001).

Estimations for NGC 253 yield $n(H_2)\sim(1-2)\times10^4$ cm^{-3} and $T_k\sim100-200$ K, which are very similar to previously published results, utilizing several molecular species (Wall et al. 1991; Paglione et al. 1995; Bradford et al. 2003; Bayet et al. 2004), but rather higher than those derived using only ^{12}CO lines (Güsten et al. 2006). For NGC 6946, our estimations suggest that $n(H_2)\sim(6-9)\times10^3$ cm^{-3} and $T_k\sim100-200$ K, which are similar to the values obtained by Meier & Turner (2004) using various CO lines including isotopes and also HCN(1-0) line, but rather higher than those derived by Walsh et al. (2002), which only made use of the CO lines (including isotopes).

The above comparisons indicate that our approach tends to yield higher densities and temperatures than other studies using only the ^{12}CO lines or even the CO isotopes. This is because our methodology makes extensive use of both the high density tracer HCN(1-0) line and the optically thin and therefore temperature dependent tracer ^{13}CO(1-0) line. In particular, HCN(1-0)/^{13}CO(1-0) is sensitive to both density and temperature, once it attains a value of around unity or higher (see Paper I for more detailed discussions). We therefore concluded that the combinations of these three line ratios, or even HCN(1-0)/^{13}CO(1-0) by itself, can effectively distinguish

Table 6. IRAS data and infrared flux ratios of sample galaxies.

Galaxy	$\log \frac{f(12\ \mu m)}{f(25\ \mu m)}$	$\log \frac{f(12\ \mu m)}{f(60\ \mu m)}$	$\log \frac{f(12\ \mu m)}{f(100\ \mu m)}$	$\log \frac{f(25\ \mu m)}{f(60\ \mu m)}$	$\log \frac{f(25\ \mu m)}{f(100\ \mu m)}$	$\log \frac{f(60\ \mu m)}{f(100\ \mu m)}$
NGC 253	-0.5762 ± 0.0004	-1.3726 ± 0.0001	-1.4968 ± 0.0004	-0.7964 ± 0.0001	-0.9206 ± 0.0003	-0.1242 ± 0.0002
NGC 2146	-0.4400 ± 0.0016	-1.3320 ± 0.0005	-1.4535 ± 0.0015	-0.8920 ± 0.0007	-1.0135 ± 0.0009	-0.1215 ± 0.0006
NGC 2903	-0.2131 ± 0.0045	-1.0586 ± 0.0018	-1.3919 ± 0.0029	-0.8455 ± 0.0035	-1.1789 ± 0.0035	-0.3333 ± 0.0008
M82	-0.6220 ± 0.0002	-1.2704 ± 0.00005	-1.2379 ± 0.0003	-0.6484 ± 0.00007	-0.6159 ± 0.0002	$+0.0325 \pm 0.0002$
NGC 3504	-0.5600 ± 0.0125	-1.2857 ± 0.0034	-1.4868 ± 0.0116	-0.7257 ± 0.0049	-0.9268 ± 0.0049	-0.2011 ± 0.0015
NGC 6946	-0.2328 ± 0.0013	-1.0301 ± 0.0007	-1.3803 ± 0.0013	-0.7972 ± 0.0007	-1.1475 ± 0.0009	-0.3502 ± 0.0007
NGC 6951	-0.2073 ± 0.0053	-1.0835 ± 0.0029	-1.4938 ± 0.0049	-0.8761 ± 0.0029	-1.2864 ± 0.0034	-0.4103 ± 0.0020
NGC 4736	-0.0810 ± 0.0055	-1.1495 ± 0.0040	-1.3767 ± 0.0048	-1.0685 ± 0.0029	-1.2956 ± 0.0029	-0.2271 ± 0.0009
NGC 4826	-0.0835 ± 0.0105	-1.1918 ± 0.0048	-1.5390 ± 0.0057	-1.1083 ± 0.0089	-1.4556 ± 0.0089	-0.3473 ± 0.0011
NGC 5195[†]	-0.4645 :	-1.6383 :	-1.9512 :	-1.1738 :	-1.4874 :	$-0.3135 : \pm 0.0228$

Notes.
Flux data are taken from Sanders et al. (2003).
[†] A value with a colon (":") indicates that the value has a large uncertainty.

galaxies with warm and dense molecular gas from galaxies without.

5.1.2. PDR Model

We also calculated HCN(1-0)/^{13}CO(1-0) with the PDR model. It turns out that the PDR model can also yield a HCN/^{13}CO of around unity; it requires an interstellar radiation field (ISRF) strength of around several $\times 10^3$ G_0 and a density of around several $\times 10^5$ cm^{-3}. In other words, dense molecular gas irradiated by radiation from massive stars can reproduce a high HCN/^{13}CO of around unity. The ratio decreases with decreasing ISRF strength or density, but the decrease of the ratio is sensitive to the density decrease than to the ISRF strength decrease.

Using this PDR model, the ISRF strength and the density for the starburst sample are estimated as around 10^{2-3} G_0 and on the order of 10^5 cm^{-3}, respectively. The non-starburst sample, on the other hand, has lower ISRF of the order of 10^2 G_0 and lower density of the order of 10^4 cm^{-3} or less.

The strength of the ISRF can be derived also from the IR characteristics. The range of the ISRF strength in nearby galaxies is $\sim 10^{2-4}$ G_0 (Negishi et al. 2001; Malhotra et al. 2001), and exhibits a tight correlation with the IR flux ratios between 60 μm and 100 μm, $f(60\ \mu m)/f(100\ \mu m)$; higher the ratio, higher the ISRF strength (Negishi et al. 2001). Our sample galaxies (both starburst and non-starburst samples) have a wide range of $f(60\ \mu m)/f(100\ \mu m)$, and our starburst sample has a tendency of higher ratio than that of the non-starburst sample, although the range is overlapping with the non-starburst galaxy sample (see Fig. 1 and Table 6). If we adopt the correlation shown by Negishi et al. (2001), our starburst sample has higher ISRF strength of the order of 10^{2-3} G_0 than the non-starburst sample of the order of 10^2 G_0. Those values are consistent with the values derived from HCN/^{13}CO using the PDR model, suggesting that there is a correlation between HCN/^{13}CO and $f(60\ \mu m)/f(100\ \mu m)$. In the next subsection, we study this relation, and the relations between HCN/^{13}CO and other IR flux ratios.

5.2. Relation between Molecular Gas and Dust

Dust in galaxies absorbs the radiation from stars, in particular massive stars, and re-radiate at IR wavelengths. The IR emission from galaxies, especially IR flux ratios, is therefore a good tracer for star formation activities (e.g., Helou 1986; see also reviews of Soifer et al. 1987 and Telesco 1993). The spectral energy distribution study using the IRAS and the Infrared Space Observatory (ISO) data between 3 and 1100 μm further confirmed the utility of the IR flux ratios for tracing star formation activities, and also suggested that the mid-IR continuum flux at a range of 20 – 42 μm can be the optimum dust emission tracer for current star formation activities (Dale et al. 2001). Here we compare HCN/^{13}CO and IR continuum flux ratios to ascertain the relation between molecular gas and dust properties.

In this study, we use the IRAS flux (Sanders et al. 2003) for the infrared flux due to the following reasons: (1) The IRAS data are still the only all-sky survey results so far, and all the wavelength data exist for all our sample galaxies. (2) Although the beam size of the IRAS data is large (arcminutes scale), most far-IR radiation from nearby galaxies is concentrated in the central $\sim 30''$ (Smith & Harvey 1996). The regions that traced by our observations and that by the IRAS are therefore more or less similar. Indeed, previously published single dish molecular gas studies derived important results using the IRAS data. The IRAS flux ratios for our sample galaxies are tabulated in Table 6.

Since $f(12\ \mu m)/f(25\ \mu m)$ and $f(60\ \mu m)/f(100\ \mu m)$ are good tracers of star formation (see Sect. 2 and Fig. 1), and the relation between HCN/^{13}CO and $f(60\ \mu m)/f(100\ \mu m)$ is suggested in the previous subsection, we first compare HCN/^{13}CO with these IR ratios (Fig. 6a, b). HCN/^{13}CO indeed exhibits a correlation with $f(60\ \mu m)/f(100\ \mu m)$. There exists also a correlation between HCN/^{13}CO and $f(12\ \mu m)/f(25\ \mu m)$ ratio, which is natural since $f(12\ \mu m)/f(25\ \mu m)$ correlates with $f(60\ \mu m)/f(100\ \mu m)$ (Helou 1986; Dale et al. 2001). In addition, the correlation is much tighter than the case with $f(60\ \mu m)/f(100\ \mu m)$, except for NGC 5195 that has a large uncertainty in the IR flux (see Table 6).

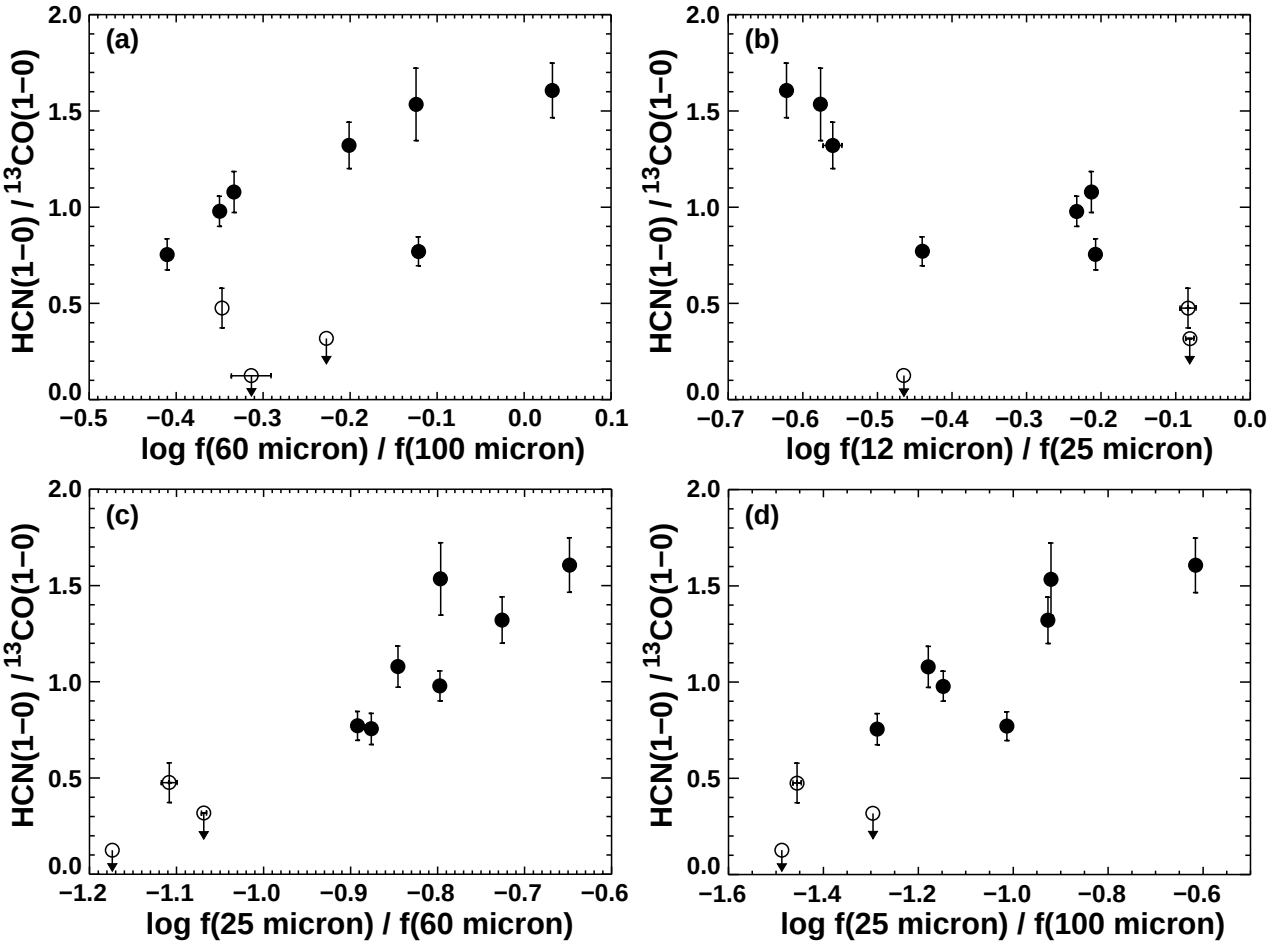

Fig. 6. Correlation diagrams between the HCN(1 – 0)/^{13}CO(1 – 0) integrated intensity ratios and (a) $f(60\ \mu\mathrm{m})/f(100\ \mu\mathrm{m})$, (b) $f(12\ \mu\mathrm{m})/f(25\ \mu\mathrm{m})$, (c) $f(25\ \mu\mathrm{m})/f(60\ \mu\mathrm{m})$, and (d) $f(25\ \mu\mathrm{m})/f(100\ \mu\mathrm{m})$ IR flux ratios. Filled and open circles are the same as in Fig. 1. Downward arrows denote upper limits. All the diagrams, especially (b), (c), and (d), exhibit tight correlations.

In Fig. 6(c) and (d), we also included correlation diagrams for $f(25\ \mu\mathrm{m})/f(60\ \mu\mathrm{m})$ and $f(25\ \mu\mathrm{m})/f(100\ \mu\mathrm{m})$, and both show tight correlations as seen in the HCN/^{13}CO – $f(12\ \mu\mathrm{m})/f(25\ \mu\mathrm{m})$ diagram. On the other hand, there is no significant correlation with other IR flux ratios, namely $f(12\ \mu\mathrm{m})/f(60\ \mu\mathrm{m})$ and $f(12\ \mu\mathrm{m})/f(100\ \mu\mathrm{m})$ (diagrams not shown).

The tight correlations between HCN/^{13}CO and the 25 μm related IR flux ratios indicate that the increase of the 25 μm continuum flux relative to the other IR continuum bands is tightly correlated with the increase of HCN/^{13}CO. Under the LVG model, HCN/^{13}CO is sensitive to molecular gas that has a temperature of 100 K or more. Under the PDR model, HCN/^{13}CO is sensitive to the molecular gas density and the strength of the ISRF. The increase of the 25 μm continuum flux is mainly due to the increase of flux from very small grains (Dale et al. 2001). It is believed that the heating of these grains is intermediate between thermal equilibrium and single-photon heating, and the increase in flux is closely related to the increase in the heating intensity of the ISRF (Dale et al. 2001). This is consistent with the results from the PDR model. Furthermore, the black body temperature around 25 μm is around 100 K or more, therefore dust needs to be heated up to approximately this temperature before achieving thermal equilibrium, in complete agreement with the results from the LVG model. The tight correlations therefore suggest that the molecular gas and dust are localized in the same regions, with the strong radiation from starburst activities heating the dust and in turn the molecular gas. With the dust heated up to around 100 K or more, the molecular gas will follow suit. In either LVG or PDR model, this tight correlation suggests that HCN/^{13}CO will be an excellent tracer for starburst conditions. It also applies that either or both the LVG and PDR mechanisms play important roles in star forming regions.

It is now well established that the amount of dense molecular gas is closely correlated to star formation activities (Solomon et al. 1992; Gao & Solomon 2004a; Gao & Solomon 2004b). Our results suggests that in addition to the amount of dense molecular gas, the amount of dense *and warm* molecular gas is also pertinent to star formation activities. The possible causes of this correlation

are the heating of molecular gas due to strong radiation and stellar wind from newly formed massive stars, and/or numerous supernova explosions.

6. Conclusion

We conducted a survey of ^{12}CO(1 – 0), ^{13}CO(1 – 0), and HCN(1 – 0) lines toward seven starburst and three non-starburst galaxies nearby using the Nobeyema 45 m telescope (beam size $\sim 14'' - 18''$). The ^{13}CO(1 – 0) and HCN(1 – 0) lines were obtained for all the sample galaxies, but the ^{12}CO(1 – 0) data for starburst galaxy samples and the HCN data for non-starburst galaxy samples were obtained from previously published data.

- The ^{13}CO(1 – 0) and HCN(1 – 0) intensities in the central regions of the starburst galaxy samples are more or less similar, with the HCN/^{13}CO integrated intensity ratios ranging between 0.75 – 1.61 (average $= 1.15 \pm 0.32$). The ^{13}CO(1 – 0) intensities in the non-starburst galaxy samples are always stronger than the HCN(1 – 0) intensities, and HCN/^{13}CO yield obviously smaller values of $< 0.31 \pm 0.14$ than for the starburst galaxy samples. We observed multiple positions for the starburst galaxy M82, and the ratios far from the center (i.e., disk region) are similar to those in the non-starburst galaxy samples.
- ^{12}CO/^{13}CO and HCN/^{12}CO also show higher values for about a factor of two in starburst galaxy samples than those in the non-starburst galaxy sample.
- The physical attributes of molecular gas derived from the line ratios under the LVG model indicate dense ($> 5 \times 10^3$ cm^{-3}) and warm ($\gtrsim 100$ K) conditions in most of the central regions of the starburst galaxy samples, but diffuse ($\lesssim 4 \times 10^3$ cm^{-3}) and cold ($\lesssim 60$ K) conditions in the non-starburst galaxy samples. Under the PDR model, this suggests that the dense molecular gas ($\sim 10^5$ cm^{-3}) is being irradiated by ISRF of 10^{2-3} G_0 in the starburst galaxy samples, but lower density molecular gas of $\lesssim 10^4$ cm^{-3} is being irradiated by lower intensity ISRF of 10^2 G_0 in the non-starburst galaxy samples.
- HCN/^{13}CO exhibits tight correlations with the IRAS flux ratios between 25 μm and other wave bands, namely, the increase of HCN/^{13}CO is related to the increase of the IRAS 25 μm flux. Since the IRAS 25 μm flux is a good tracer for star formation activities, these correlations indicate that HCN/^{13}CO is also a good tracer for star formation activities. High HCN/^{13}CO larger than unity points to dense and warm molecular gas with the temperature of 100 K or more under the LVG model, or irradiated by strong ISRF under the PDR model. The high 25 μm flux also indicates high ISRF and high dust temperature of around 100 K or more. These results suggest that molecular gas and dust are localized in the same regions in a well mixed configuration, and that the strong radiation heats up the dust and therefore the molecular gas nearby indirectly. This strong radiation also affects the molecular gas itself.

We are grateful to the NRO staff for the operation and improvement of the Nobeyama 45 m telescope. This work is supported by the National Science Council (NSC) of Taiwan, NSC 96-2112-M-001-009 and NSC 97-2112-M-001-021-MY3.

References

Aalto, S., Black, J. H., Johansson, L. E. B., & Booth, R. S. 1991, A&A, 249, 323
Aalto, S., Booth, R. S., Black, J. H., & Johansson, L. E. B. 1995, A&A, 300, 369
Alonso-Herrero, A., Ryder, S. D., & Knapen, J. H. 2001, MNRAS, 322, 757
Armus, L., Heckman, T. M., Weaver, K. A., & Lehnert, M. D. 1995, ApJ, 445, 666
Barth, A. J., Ho, L. C., Filippenko, A. V., & Sargent, W. L. W. 1995, AJ, 110, 1009
Bayet, E., Gerin, M., Phillips, T. G., & Contursi, A. 2004, A&A, 427, 45
Bradford, C. M., Nikola, T., Stacy, G. J., Bolatto, A. D., Jackson, J. M., Savage, M. L., Davidson, J. A., & Higdon, S. J. 2003, ApJ, 586, 891
Braine, J., Combes, F., Casoli, F., Dupraz, C., Gérin, M., Klein, U., Wielebinski, R., & Brouillet, N. 1993, A&A, 97, 887
Brouillet, N., Muller, S., Herpin, F., Braine, J., & Jacq, T. 2005, A&A, 429, 153
Burton, W. B., & Gordon, M. A. 1978, A&A, 63, 7
Casoli, F., Dupraz, C., & Combes, F. 1992, A&A, 264, 55
Condon, J. J., Condon, M. A., Gisler, G., & Puschell, J. J. 1982, ApJ, 252, 102
Condon, J. J., Helou, G., Sanders, D. B., & Soifer, B. T. 1990, ApJS, 73, 359
Dale, A. D., Helou, G., Contursi, A., Silbermann, N. A., & Kolhatkar, S. 2001, ApJ, 549, 215
Della Ceca, R., Griffiths, R. E., Heckman, T. M., Lehnert, M. D., & Weaver, K. A. 1999, ApJ, 514, 772
Devereux, N. 1989, ApJ, 346, 126
Devereux, N., Taniguchi, Y., Sanders, D. B., Nakai, N., & Young, J. S. 1994, AJ, 107, 2006
Drozdovsky, I. O., & Karachentsev, I. D. 2000, A&AS, 142, 425
Dumke, M., Nieten, Ch., Thuma, G., Wielebinski, R., & Walsh W. 2001, A&A, 373, 853
Elmegreen, D. M., Chromey, F. R., & Santos, M. 1998, AJ, 116, 1221
Elmegreen, D. M., Chromey, F. R., Sawyer, J. E., & Reinfeld, E. L. 1999, AJ, 118, 777
Engelbracht, C. W., Rieke, M. J., Rieke, G. H., & Latter, W. B. 1996, ApJ, 467, 227
Feldmeier, J. J., Ciardullo, R., & Jacoby, G. H. 1997, ApJ, 479, 231
Flower, D. R., & Launay, J. M. 1985, MNRAS, 214, 271
Gao, Y., & Solomon, P. M. 2004a, ApJS, 152, 63
Gao, Y., & Solomon, P. M. 2004b, ApJ, 606, 271
Goldreich, P., & Kwan, J. 1974, ApJ, 189, 441

González-Delgado, R. M., Pérez, E., Tadhunter, C., Vilchez, J. M., & Rondríguez-Espinosa, J. M. 1997, ApJS, 108, 155
Green, S., & Thaddeus, P. 1974, ApJ, 191, 653
Greenawalt, B., Walterbos, R. A. M., Thilker, D., & Hoopes, C. G. 1998, ApJ, 506, 135
Güsten, R., Philipp, S. D., Weiß, A., & Klein, B. 2006, A&A, 454, L115
Hafok, H., & Stutzki, J. 2003, A&A, 398, 959
Helfer, T. T., & Blitz, L. 1997, ApJ, 478, 233
Helou, G. 1986, ApJL, 311, L33
Ho, L. C., Filippenko, A. V., & Sargent, W. L. W. 1995, ApJS, 98, 477
Ho, L. C., Filippenko, A. V., & Sargent, W. L. W. 1997, ApJS, 112, 315
Hummel, E., van der Hulst, J. M., Keel, W. C., & Kennicutt Jr., R. C. 1987, A&AS, 70, 517
Inui, T., Matsumoto, H., Tsuru, T. G., Koyama, K., Matsushita, S., Peck, A. B., & Tarchi, A. 2005, PASJ, 57, 135
Irvine, W. M., Goldsmith, P. F., & Hjalmarson, A. 1987, in Interstellar Processes, ed. D. J. Hollenbach & H. A. Thronson (Dordrecht: Reidel), 561
Jackson, J. M., Heyer, M. H., Paglione, T. A. D., & Bolatto, A. D. 1996, ApJL, 456, L91
Karachentsev, I. D., Sharina, M. E., & Huctmeier, W. K. 2000, A&A, 362, 544
Kennicutt Jr., R. C. 1998, ApJ, 498, 541
Keto, E., Ball, R., Arens, J., Jernigan, G., Meixner, M., Skinner, C., & Graham, J. 1993, ApJL, 413, L23
Kohno, K. 1998, Ph.D. Thesis, University of Tokyo
Kohno, K., Kawabe, R., & Vila-Vilaró, B. 1999, ApJ, 511, 157
Kohno, K., Tosaki, T., Matsushita, S., Vila-Vilaó, B., Shibatsuka, T., & Kawabe, R. 2002, PASJ, 54, 541
Kuno, N., Nishiyama, K., Nakai, N., Sorai, K., Vila-Vilaró, B., & Handa, T. 2000, PASJ, 52, 775
Kuno, N., et al. 2007, PASJ, 59, 117
Lada, E. A. 1992, ApJL, 393, L25
Malhotra, S., et al. 2001, ApJ, 561, 766
Matsushita, S., et al. 2004, ApJL, 616, L55
Matsushita, S., Kawabe, R., Kohno, K., Matsumoto, H., Tsuru, T. G., & Vila-Vilaró, B. 2005, ApJ, 618, 712
Matsushita, S., Kohno, K., Vila-Vilaró, B., Tosaki, T., & Kawabe, R. 1998, ApJ, 495, 267 (Paper I)
Matsushita, S., Kohno, K., Vila-Vilaró, B., Tosaki, T., & Kawabe, R. 1999, Adv. Space Res., 23, 1015
McKee, C. F., Storey, J. W. V., Watson, D. W., & Green, S. 1982, ApJ, 259, 647
Meier, D. S., & Turner, J. L. 2004, AJ, 127, 2069
Meijerink, R., & Spaans, M. 2007, A&A, 436, 397
Meijerink, R., Spaans, M., & Israel, F. P. 2007, A&A, 461, 793
Nakai, N., Hayashi, M., Handa, T., Sofue, Y., & Hasegawa, T. 1987, PASJ, 39, 685
Negishi, T., Onaka, T., Chan, K.-W., & Roellig, T. L. 2001, A&A, 375, 566
Paglione, T. A. D., Tosaki, T., & Jackson, J. M. 1995, ApJL, 454, L117
Paglione, T. A. D., et al. 2001, ApJS, 135, 183
Petitpas, G. R., & Wilson, C. D. 2000, ApJL, 538, L117
Pritchet, C. 1977, ApJS, 35, 397
Rekola, R., Richer, M. G., McCall, M. L., Valtonen, M. J., Kotilainen, J. K., & Flynn, C. 2005, MNRAS, 361, 330
Reynaud, D., & Downes, D. 1999, A&A, 347, 37
Rieke, G. H. 1988, in Galactic and Extragalactic Star Formation, ed. R. E. Pudrits, & M. Fich, (Dordrecht: Kluwer), 561
Rieke, G. H., Lebofsky, M. J., Thompson, R. I., Low, F. J., & Tokunaga, A. T. 1980, 238, 24
Rieke, G. H., Lebofsky, M. J., & Walker, C. E. 1988, 325, 679
Sage, L. J., & Isbell, D. W. 1991, A&A, 247, 320
Saikia, D. J., Pedler, A., Unger, S. W., & Axon, D. J. 1994, MNRAS, 270, 46
Sakai, S., & Madore, B. F. 1999, ApJ, 526, 599
Sakamoto, K., et al. 2006, ApJ, 636, 685
Sanders, D. B., Scoville, N. Z., & Soifer, B. T. 1991, ApJ, 370, 158
Sanders, D. B., Mazzarella, J. M., Kim, D.-C., Surace, J. A., & Soifer, B. T. 2003, AJ, 126, 1607
Sauvage, M., et al. 1996, A&A, 315, L89
Scoville, N. Z., & Solomon, P. M. 1974, ApJL, 187, L67
Sérsic, J. L. 1973, PASP, 85, 103
Sérsic, J. L., & Pastoriza, M. 1965, PASP, 77, 287
Sérsic, J. L., & Pastoriza, M. 1967, PASP, 79, 152
Shen, J., & Lo, K. Y. 1995, ApJL, 445, L99
Shioya, Y., Tosaki, T., Ohyama, Y., Murayama, T., Yamada, T., Ishizuki, S., & Taniguchi, Y. 1998, PASJ, 50, 317
Smith, B. J., & Harvey, P. M. 1996, ApJ, 468, 139
Soifer, B. T., Houck, J. R., & Neugebauer, G. 1987, ARA&A, 25, 187
Solomon, P. M., Scoville, N. Z., & Sanders, D. B. 1979, ApJL, 232, L89
Solomon, P. M., Downes, D., & Radford, S. J. E. 1992, ApJL, 387, L55
Sorai, K., Nakai, N., Kuno, N., & Nishiyama, K. 2002, PASJ, 54, 179
Sorai, K., Nakai, N., Kuno, N., Nishiyama, K., & Hasegawa, T. 2000, PASJ, 52, 785
Spergel, D. N. & Blitz, L. 1992, Nature, 357, 665
Strickland, D. K., Heckman, T. M., Colbert, E. J., Hoopes, C. G., & Weaver, K. A. 2004, ApJ, 606, 829
Taniguchi, Y., Ohyama, Y., Yamada, T., Mouri, H., & Yoshida, M. 1996, ApJ, 467, 215
Telesco, C. M. 1993, in Infrared Astronomy, ed. A. Mampaso, M. Prieto, & F. Sánchez (Cambridge: Cambridge University Press), 173
Telesco, C. M., & Harper, D. A. 1980, ApJ, 235, 392
Tosaki, T., & Shioya, Y. 1997, ApJ, 484, 664
Tsai, A.-L., et al. 2009, PASJ, 61, 237
Tully, R. B. 1988, Nearby Galaxies Catalog (Cambridge: Cambridge University Press)
Turner, J. L., & Ho, P. T. P. 1983, ApJL, 268, L79
Turner, J. L., & Ho, P. T. P. 1994, ApJ, 421, 122
Ulich, B. L., & Haas, R. W. 1976, ApJS, 30, 247
Valentini, G., et al. 2003, ApJ, 595, 779
Walker, C. E., Lebofsky, M. J., & Rieke, G. H. 1988, ApJ, 325, 687
Wall, W. F., Jaffe, D. T., Israel, F. P., & Bash, F. N. 1991, ApJ, 380 384
Walsh, W., Beck, R., Thuma, G., Weiß, A., Wielebinski, R., & Dumke, M. 2002, A&A, 388, 7
Warner, J. W. 1974, ApJ, 190, 19
Weiß, A., Neininger, N., Hüttemeister, S., & Klein U. 2001, A&A, 365, 571
Wozniak, H., Friedli, D., Martinet, L., Martin, P., & Bratschi, P. 1995, A&AS, 111, 115
Wynn-Williams, C. G., & Becklin, E. E. 1985, ApJ, 290, 108

Young, J. S., Allen, L., Kenney, J. D. P., Lesser, A., & Rownd, B. 1996, AJ, 112, 1903
Young, J. S., & Scoville, N. Z. 1991, ARA&A, 29, 581